

Non-Linear Model for Compression Tests on Articular
Cartilage

Original

Non-Linear Model for Compression Tests on Articular

Cartilage / Grillo, Alfio; A., Guaily; Giverso, Chiara; S., Federico. - In: JOURNAL OF BIOMECHANICAL ENGINEERING.
- ISSN 0148-0731. - STAMPA. - 137:(2015), pp. 071004-1-071004-8. [10.1115/1.4030310]

Availability:

This version is available at: 11583/2603775 since: 2020-05-28T12:43:06Z

Publisher:

New York, N.Y.: American Society of Mechanical Engineers <http://www.asme.org>,

Published

DOI:10.1115/1.4030310

Terms of use:

This article is made available under terms and conditions as specified in the corresponding bibliographic description in the repository

Publisher copyright

(Article begins on next page)

NON-LINEAR MODEL FOR COMPRESSION TESTS ON ARTICULAR CARTILAGE

Alfio Grillo

Dept of Mathematical Sciences “G. Lagrange”
Politecnico di Torino
Corso Duca degli Abruzzi 24
10124, Torino, Italy
Email: alfio.grillo@polito.it

Chiara Givero

Modelling and Scientific Computing (MOX)
Politecnico di Milano,
Via Bonardi 9, 20133, Milan, Italy
Fondazione CEN
Piazza Leonardo da Vinci 32, 20133, Milan, Italy
Email: chiara.givero@polimi.it

Amr Guaily

Engineering Mathematics and Physics Dept
Cairo University
Cairo University Rd
12613, Giza, Egypt
Email: a.guaily@eng.cu.edu.eg

Salvatore Federico*

Dept of Mechanical and Manufacturing Engineering
The University of Calgary
2500 University Drive NW
Calgary, Alberta, T2N1N4, Canada
Email: salvatore.federico@ucalgary.ca

ABSTRACT

Hydrated soft tissues, such as articular cartilage, are often modelled as biphasic systems with individually incompressible solid and fluid phases, and biphasic models are employed to fit experimental data in order to determine the mechanical and hydraulic properties of the tissues. Two of the most common experimental setups are confined and unconfined compression. Analytical solutions exist for the unconfined case with the linear, isotropic, homogeneous model of articular cartilage, and for the confined case with the non-linear, isotropic, homogeneous model. The aim of this contribution is to provide an easily implementable numerical tool to determine a solution to the governing differential equations of (homogeneous and isotropic) unconfined and (inhomogeneous and isotropic) confined compression under large deformations. The large-deformation governing equations are reduced to equivalent diffusive equations, which are then solved by means of Finite Difference methods. The solution strategy proposed here could be used to generate benchmark tests for validating complex user-defined material models within Finite Element implementations, and for determining the tissue’s mechanical and hydraulic properties from experimental data.

1 Introduction

Since its introduction, the biphasic model of articular cartilage [1–3] has been the standard manner to study also other hydrated soft tissues. In this model, cartilage is represented as the mixture of an incompressible solid, representing structural macromolecules such as collagen fibres and proteoglycans, and an incompressible fluid, representing the interstitial water, along with the various chemical species dissolved in it. In order to fully characterise the behaviour of cartilage according to the biphasic model, it is necessary to experimentally evaluate its elastic properties and its permeability (which is the parameter accounting for the solid-fluid interaction). The most common tests are confined and unconfined compression. In the former, a cartilage sample is placed in an impermeable, rigid chamber and compressed by a porous, rigid piston, so that the fluid can escape from the sample through the piston. In the latter, cartilage is squeezed between two impermeable, rigid plates, so that it can freely expand laterally and fluid can freely escape through the lateral boundary.

Aside from many studies based on Finite Element Analysis, confined and unconfined compression have been also modelled analytically in some particular cases. Based on the linear biphasic model of articular cartilage [1–3], Armstrong et al. [4] derived

*Address all correspondence to this author.

an analytical solution for the unconfined compression test under small deformations, in terms of series expansions. Holmes and Mow [5] proposed an isotropic homogeneous model of articular cartilage, with non-linear elasticity and deformation-dependent permeability, and studied the case of confined compression analytically. Moreover, in a previous work [6], unconfined compression has been solved numerically under small deformations for a linear, isotropic, inhomogeneous model. However, these specific cases cannot be used to describe many experimental set-up conditions.

In this work, based on the large-strain governing equations of a biphasic mixture (e.g., [7–9]), we propose a solution to the differential equations of both unconfined and confined compression problems under large deformations, with isotropic non-linear elasticity and deformation-dependent permeability [5]. The case of unconfined compression is studied under the hypothesis of homogeneity, whereas in that of confined compression the elastic properties and permeability are inhomogeneous, as obtained from published experimental works [10, 11], and similarly to what has been done in [6] for the small-deformation case.

Once the hyperelastic constitutive equations are set, the governing equations consist of a system of 4 differential equations in 4 unknowns: three components of the configuration map (treated in terms of their derivatives, i.e., the components of the deformation gradient tensor), and the fluid pressure. For the cases of homogeneous unconfined compression and inhomogeneous confined compression, the material gradient of the pressure is eliminated, yielding a single scalar equation in the volume ratio of the diffusion-advection type, which simplifies remarkably the mathematical problem. The solution that we propose is obtained numerically via a direct application of Finite Difference schemes, and can be used as a rapid, yet effective, comparison solution to verify the robustness and accuracy of complex user-defined material models within Finite Element methods. Furthermore, the proposed implementation is easily manageable and makes the code potentially useful in the determination of mechanical parameters, directly fitting experimental curves.

2 Balance Laws

Here, the description of articular cartilage is limited to the macro-scale, which is interpreted as the laboratory scale at which constitutive information on the overall mechanical behaviour of a given sample of tissue is extracted by means of experiments. At this scale, the tissue is modelled as a biphasic mixture comprising a solid and a fluid phase. The solid phase is the macro-scale representation of a deformable porous medium, which, in fact, is itself a mixture composed mainly of proteoglycans and collagen fibres. The fluid phase represents the interstitial fluid, which occupies the voids of the porous medium and consists mainly of water, ions and various types of chemical compounds, such as nutrients for the cells and byproducts of the cellular metabolism [12].

In the following, the subscripts ‘s’ and ‘f’ shall specify whether a given physical quantity is associated with the solid or with the fluid phase. When there is no danger of confusion, the terms “phase” and “constituent” shall be used interchangeably. The mass distribution of the α th phase of the mixture ($\alpha = f, s$), can be expressed either per unit volume occupied by the α th phase itself, or per unit volume of the mixture as a whole. In the first case, one speaks of the “true”, or intrinsic, mass density ρ_α of the α th phase. In the second case, instead, one introduces the “apparent” mass density $\phi_\alpha \rho_\alpha$, with ϕ_α being the volumetric fraction of the α th phase, i.e., the ratio between the size of the volume occupied by α th phase and the size of a representative volume for the mixture as a whole. Note that the mixture is subjected to the saturation constraint $\phi_s + \phi_f = 1$. All the balance laws referred to the macro-scale description of the mixture’s constituents are formulated by employing the apparent mass densities of the phases.

In the absence of sources and sinks of mass, the spatial, local form of the mass balance laws associated with the fluid and the solid phase can be written as

$$\partial_t(\phi_f \rho_f) + \text{div}(\phi_f \rho_f \mathbf{v}_s) + \text{div}(\rho_f \mathbf{w}) = 0, \quad (1a)$$

$$\partial_t(\phi_s \rho_s) + \text{div}(\phi_s \rho_s \mathbf{v}_s) = 0, \quad (1b)$$

where \mathbf{v}_s and \mathbf{v}_f are the velocities of the solid and fluid phase, respectively, and $\mathbf{w} = \phi_f(\mathbf{v}_f - \mathbf{v}_s)$ is the filtration velocity. For more details on the kinematics of biphasic mixtures, see, for instance, [13]. From here on, the mass densities ρ_f and ρ_s are assumed to be given constants, which means that both the fluid and the solid phases are regarded as intrinsically incompressible materials. By definition, this means that the substantial derivatives $D_\alpha \rho_\alpha := \partial_t \rho_\alpha + (\text{grad} \rho_\alpha) \mathbf{v}_\alpha$ are zero for $\alpha = f, s$.

Under the assumption of negligible inertial effects, in the absence of body forces external to the considered mixture, and accepting the validity of Darcy’s law, the spatial, local balance laws of momentum associated with the mixture as a whole and the fluid phase can be written as

$$\mathbf{0} = \text{div}(\boldsymbol{\sigma}_f + \boldsymbol{\sigma}_s), \quad (2)$$

$$\mathbf{w} = -\mathbf{k} \text{grad} p, \quad (3)$$

where $\boldsymbol{\sigma}_f$ and $\boldsymbol{\sigma}_s$ are the Cauchy stress tensors of the fluid and solid phase, respectively, and \mathbf{k} is the spatial permeability tensor. The mixture is assumed to be closed with respect to momentum.

If the fluid phase is modelled as an incompressible and macroscopically inviscid Stokes fluid, the stress tensors for the

111 fluid, the solid and the whole tissue admit the expressions

$$\boldsymbol{\sigma}_f = -\phi_f p \mathbf{g}^{-1}, \quad (4a)$$

$$\boldsymbol{\sigma}_s = -\phi_s p \mathbf{g}^{-1} + \boldsymbol{\sigma}_c, \quad (4b)$$

$$\boldsymbol{\sigma} = \boldsymbol{\sigma}_f + \boldsymbol{\sigma}_s = -p \mathbf{g}^{-1} + \boldsymbol{\sigma}_c, \quad (4c)$$

112 where $\boldsymbol{\sigma}_c$ is referred to as the *constitutive part* of $\boldsymbol{\sigma}_s$, p is the hy-
113 drostatic pressure, and \mathbf{g}^{-1} , with components g^{ab} , is the inverse
114 of the spatial metric tensor \mathbf{g} and serves here as the “contravari-
115 ant” identity tensor.

116 The deformation of the solid phase is denoted by χ , the de-
117 formation gradient by \mathbf{F} (with components $F^a_A = \chi^{a,A}$), and the
118 volume ratio by $J = \det \mathbf{F}$. By performing a backward Piola
119 Transformation of (1a) and (1b), which is done by multiplying
120 both equations by J , one obtains

$$\dot{\phi}_{fR} + \text{Div}(\mathbf{W}) = 0, \quad (5a)$$

$$\dot{\phi}_{sR} = 0. \quad (5b)$$

121 In (5a) and (5b), the superimposed dot stands for time differenti-
122 ation, Div is the material divergence operator, and

$$\phi_{sR} = J \phi_s, \quad (6a)$$

$$\phi_{fR} = J \phi_f = J - \phi_{sR}, \quad (6b)$$

$$\mathbf{W} = J \mathbf{F}^{-1} \mathbf{w} = -\mathbf{K} \text{Grad } p, \quad (6c)$$

123 with $\mathbf{K} = J \mathbf{F}^{-1} \mathbf{k} \mathbf{F}^{-T}$ being the material permeability tensor, are
124 the Piola transforms of ϕ_f , ϕ_s and \mathbf{w} . In particular, (6a) can
125 be used to express ϕ_s as a function of the volume ratio of the
126 solid phase, i.e., $\phi_s = J^{-1} \phi_{sR}$. This result, which stems from
127 the incompressibility of the solid phase, permits to rephrase the
128 inequalities $0 \leq \phi_s(x, t) \leq 1$ (with the upper bound condition
129 $\phi_s(x, t) = 1$ implying that the limit of *compaction* is reached)
130 as $0 \leq \phi_{sR}(X) \leq J(X, t)$, and thus it places on J the *unilateral*
131 constraint $J(X, t) \geq \phi_{sR}(X)$ [8]. In particular, when the condition
132 $J = \phi_{sR}$ is met at a given point X of the reference configuration
133 \mathcal{B}_R , all fluid has been expelled from the point, which thereby re-
134 mains composed of solid alone, which is incompressible by hy-
135 pothesis. It is worth to recall that, for a biphasic mixture, the re-
136 quirement that both phases are intrinsically incompressible, does
137 *not* lead to the restriction $J = 1$ of isochoric motion, due to the
138 presence of the volumetric fraction ϕ_s in (1b). Indeed, the as-
139 sumption of incompressibility, which is translated into $D_s \rho_s = 0$,
140 transforms (1b) into an equation for ϕ_s , whose variations are
141 compensated for by the change of volume of the solid phase. In
142 the material formalism, this fact is reflected by (6a), which allows
143 to express ϕ_s as a function of J . An extensive discussion about

144 this issue and, in particular, on the consequences of compaction,
145 is given in [8].

146 Finally, by adding together (5a) and (5b), using (6c), and
147 performing a Piola transformation of (2), with $\boldsymbol{\sigma}_f$ and $\boldsymbol{\sigma}_s$ given
148 by (4b) and (4a), the material form of the mass and momentum
149 balance laws becomes

$$J = \text{Div}(\mathbf{K} \text{Grad } p), \quad (7a)$$

$$\text{Div} \mathbf{P}_c = J \mathbf{g}^{-1} \mathbf{F}^{-T} \text{Grad } p, \quad (7b)$$

150 where $\mathbf{P}_c = J \boldsymbol{\sigma}_c \mathbf{F}^{-T}$ is the constitutive part of the first Piola-
151 Kirchhoff stress tensor of the solid phase. Furthermore, the first
152 Piola-Kirchhoff stress for the whole tissue is obtained by Piola-
153 transforming (4c), which yields $\mathbf{P} = -J p \mathbf{g}^{-1} \mathbf{F}^{-T} + \mathbf{P}_c$.

154 3 Constitutive Laws and Final Model Equations

155 The non-linear isotropic model proposed by Holmes and
156 Mow [5] is adopted in this work. The solid phase is regarded
157 as hyperelastic, with potential

$$\hat{W}(\mathbf{C}) = \alpha_0 (\exp[\varphi(\mathbf{C})] - 1), \quad (8a)$$

$$\varphi(\mathbf{C}) = \alpha_1 [I_1(\mathbf{C}) - 3] + \alpha_2 [I_2(\mathbf{C}) - 3] - \beta \ln [I_3(\mathbf{C})], \quad (8b)$$

158 where $\alpha_0, \alpha_1, \alpha_2$, and β are material parameters, and $I_1(\mathbf{C}) =$
159 $\text{tr}(\mathbf{C})$, $I_2(\mathbf{C}) = \frac{1}{2}[(\text{tr}(\mathbf{C}))^2 - \text{tr}(\mathbf{C}^2)]$, and $I_3(\mathbf{C}) = \det(\mathbf{C})$ are the in-
160 variants of the right Cauchy-Green deformation tensor $\mathbf{C} = \mathbf{F}^T \mathbf{F}$.
161 Thus, \mathbf{P}_c is given by

$$\mathbf{P}_c = \hat{\mathbf{P}}_c(\mathbf{F}) = \mathbf{F} \left(2 \frac{\partial \hat{W}}{\partial \mathbf{C}}(\mathbf{C}) \right). \quad (9)$$

162 The permeability is assumed to be related to J via the Holmes-
163 Mow law [5]

$$k = \hat{k}(J) = k_0 \left(\frac{J - \phi_{sR}}{1 - \phi_{sR}} \right)^\gamma \exp\left(\frac{M}{2}(J^2 - 1)\right), \quad (10)$$

164 where γ and M are material parameters, $\hat{k}(J) = k$ denotes the
165 constitutive function associated with the scalar permeability k ,
166 and $k_0 = \hat{k}(1)$ is the value of the permeability in the undeformed
167 configuration ($J = 1$). In order to satisfy (7a), \hat{k} must vanish
168 at compaction, i.e., at $J = \phi_{sR}$, so that \hat{J} vanishes too, and the
169 incompressibility constraint is respected. As an isotropic tensor-
170 valued function, the permeability is assumed to be spherical [14],
171 so that the spatial and material permeability tensors are given by

$$\mathbf{k} = k \mathbf{g}^{-1} = \hat{k}(J) \mathbf{g}^{-1}, \quad (11a)$$

$$\mathbf{K} = \hat{\mathbf{K}}(\mathbf{C}) = J \hat{k}(J) \mathbf{C}^{-1}. \quad (11b)$$

172 In (10), \hat{k} vanishes for $J = \phi_{\text{SR}}$, and therefore \mathbf{k} vanishes too. 217
 173 For an inhomogeneous material, \hat{W} and $\hat{\mathbf{K}}$ depend explicitly on 218
 174 the material point X , through the parameters $\alpha_0, \alpha_1, \alpha_2, \beta$ and 219
 175 k_0, γ, M , and possibly through ϕ_{SR} as well. Hereafter, cartilage 220
 176 is regarded as homogeneous for the case of unconfined compression 221
 177 and as inhomogeneous for the case of confined compression. 222

178 Equations (7a) and (7b) are suitable for computations based 223
 179 on the Finite Element Method (FEM), cf., e.g., [12]. Here, how- 224
 180 ever, a different approach is followed, since the aim of this work 225
 181 is to provide a valid alternative to Finite Element implementa- 226
 182 tions for the considered problems. The reason for undertaking 227
 183 this task is to supply fast estimates about the hydraulic and me- 228
 184 chanical properties of cartilage (in the limit case of isotropy), 229
 185 that can be used as reference for testing the reliability of com- 230
 186 plex, FEM-based numerical strategies, which might be necessary 231
 187 for highly non-linear, coupled, anisotropic and inhomogeneous 232
 188 problems. The first step is the decoupling of (7a) from (7b), 233
 189 which is achieved by substituting $\text{Grad } p$, obtained from (7b), 234
 190 into (7a). By accounting for (11b), this yields

$$j = \text{Div} [\hat{k}(J) \mathbf{F}^{-1} \text{Div}(\hat{\mathbf{P}}_c(\mathbf{F}))], \quad (12a)$$

$$\text{Grad } p = J^{-1} \mathbf{F}^T \mathbf{g} \text{Div}(\hat{\mathbf{P}}_c(\mathbf{F})). \quad (12b)$$

191 Equations (12a) and (12b) have some relevant differences 235
 192 with respect to the original Equations (7a) and (7b). Firstly, p can 236
 193 be computed *a posteriori* by solving (12b), once (12a) is solved 237
 194 for χ . Secondly, (12b) involves only the first-order space deriva- 238
 195 tives of p , whereas the Poisson-like equation (7a) also involves 239
 196 the second-order space derivatives of p . Finally, the permeability 240
 197 does not directly affect the pressure. Rather, it influences the solu-
 198 tion of (12a), which involves the third-order space derivatives
 199 of χ as well as its mixed derivatives (i.e., with respect to both
 200 time and space), as prescribed by the computation of J .

201 4 Axisymmetric Unconfined Compression

202 The subject of this section is the study of the unconfined
 203 compression test of a cylindrical specimen of cartilage. In this
 204 test, the specimen is assumed to be homogeneous and isotropic.
 205 Therefore, its permeability and hyperelastic potential are in-
 206 dependent of material points, and related to deformation only
 207 through the invariants of \mathbf{C} . Moreover, ϕ_{SR} is a model constant.

208 The cylindrical specimen is inserted between two rigid and
 209 impermeable plates that remain parallel to each other for the
 210 whole duration of the experiment. The lower plate is kept fixed,
 211 while the upper one moves downward according to a prescribed
 212 loading protocol. In this work, only a displacement-control test is
 213 considered. The lateral wall of the specimen is traction-free and
 214 permeable. The lower and upper surfaces of the specimen are
 215 allowed to glide on the lower and upper plate, respectively, in an
 216 axisymmetric way. Moreover, no friction is considered, so that

the specimen preserves its original cylindrical shape throughout
 the experiment.

The geometry of the specimen, its material symmetries (ho-
 mogeneity and isotropy) and the experimental protocol make
 it convenient to employ cylindrical coordinates $\{R, \Theta, Z\}$ and
 $\{r, \theta, z\}$ for both the reference (undeformed) and deformed con-
 figuration, respectively. Below, the boundary conditions for χ
 and p , which have to hold at all times, are specified for all por-
 tions of the boundary.

At the lower boundary, $(R, \Theta, Z) \in [0, R_{\text{ext}}] \times [0, 2\pi] \times \{0\}$,

$$\chi^z = 0, \quad [\text{no displacement}] \quad (13a)$$

$$(-\mathbf{K} \text{Grad } p) \cdot (-\mathbf{E}_Z) = 0, \quad [\text{no flux}] \quad (13b)$$

227 where χ^z is the axial component of the deformation χ , and \mathbf{E}_Z
 228 is the unit vector pointing upward and aligned along the axial
 229 direction.

230 At the upper boundary, $(R, \Theta, Z) \in [0, R_{\text{ext}}] \times [0, 2\pi] \times \{H\}$,

$$\chi^z = \lambda_Z H, \quad (14a)$$

$$\lambda_Z(t) = 1 - \frac{u_T}{H} [1 - \exp(-t/t_u)], \quad [\text{prescribed stretch}] \quad (14b)$$

$$(-\mathbf{K} \text{Grad } p) \cdot \mathbf{E}_Z = 0, \quad [\text{no flux}] \quad (14c)$$

231 where H is the initial height of the specimen, and λ_Z is the im-
 232 posed time-dependent stretch, with target displacement u_T and
 233 time constant t_u .

234 At the lateral boundary, $(R, \Theta, Z) \in \{R_{\text{ext}}\} \times [0, 2\pi] \times [0, H]$,

$$-p = 0, \quad [\text{atmospheric pressure}] \quad (15a)$$

$$\mathbf{P} \cdot \mathbf{E}_R = \mathbf{0}, \quad [\text{traction-free boundary}] \quad (15b)$$

235 where \mathbf{E}_R is the referential radial unit vector, pointing outward
 236 and aligned along the radial direction. Finally, the axial sym-
 237 metry of the problem places the further restriction that the radial
 238 deformation and the radial fluid flux must vanish at the origin of
 239 each cross section of the specimen. Since the reference config-
 240 uration is assumed to coincide with the stress-free, undeformed
 241 one, the initial conditions $p(X, 0) = 0$ and $\chi(X, 0) = X$ apply at
 242 all inner points X of the computational domain.

243 It should be remarked that (15b) involves the overall first
 244 Piola-Kirchhoff stress tensor of the mixture as a whole. Since it
 245 holds that $\mathbf{P} = -J p \mathbf{g}^{-1} \mathbf{F}^{-T} + \mathbf{P}_c$, and pressure has to vanish on
 246 the lateral boundary of the specimen, (15b) can also be rephrased
 247 in terms of the constitutive part of \mathbf{P} , i.e. $\mathbf{P}_c \cdot \mathbf{E}_R = \mathbf{0}$.

4.1 Specific Form of the Deformation

Due to the symmetries of the problem, χ acquires the form

$$r = \chi^r(R, \Theta, Z, t) \equiv f(R, t), \quad (16a)$$

$$\vartheta = \chi^\vartheta(R, \Theta, Z, t) = \Theta, \quad (16b)$$

$$z = \chi^z(R, \Theta, Z, t) = \lambda_Z(t)Z. \quad (16c)$$

In (16a), χ^r is re-defined as a function f of R and t alone, and $\lambda_Z(t)$ is the uniform axial stretch, as defined in (14b). The latter is a function known from the boundary conditions on the displacement in the axial direction for the case of a displacement-controlled test. The stretches in the radial and circumferential direction are given by

$$\lambda_R(R, t) = \frac{\partial f}{\partial R}(R, t) \equiv f'(R, t), \quad (17a)$$

$$\lambda_\Theta(R, t) = \frac{f(R, t)}{R}. \quad (17b)$$

Thus, the matrix representation of \mathbf{F} , which is diagonal, and the volume ratio J become

$$[F^a_A](R, t) = \text{diag}[\lambda_R(R, t), \lambda_\Theta(R, t), \lambda_Z(t)], \quad (18a)$$

$$J(R, t) = f'(R, t) \frac{f(R, t)}{R} \lambda_Z(t). \quad (18b)$$

4.2 Stress and Balance Equations

Because of the deformation specified by (16a)–(16c), the matrix representation of \mathbf{P}_c is diagonal. Moreover, the equation of the balance of mass (12a), and the only non-trivially satisfied component of the equation of balance of momentum (12b) read

$$j = \left(\frac{\partial}{\partial R} + \frac{1}{R} \right) \left[\frac{\hat{k}(J)}{\lambda_R} \left(\frac{\partial P_c^{rR}}{\partial R} + \frac{P_c^{rR} - P_c^{\vartheta\Theta}}{R} \right) \right], \quad (19a)$$

$$\frac{\partial p}{\partial R} = \frac{\lambda_R}{J} \left(\frac{\partial P_c^{rR}}{\partial R} + \frac{P_c^{rR} - P_c^{\vartheta\Theta}}{R} \right). \quad (19b)$$

Since P_c^{rR} and $P_c^{\vartheta\Theta}$ are constitutive functions of λ_R , λ_Θ and λ_Z , and since λ_R and λ_Θ involve the radial deformation f , while λ_Z is known from the outset, the right-hand-side of (19a) can be recast as a combination of terms in the unknown f and its radial derivatives up the third-order. Thus, after substituting the constitutive laws, an equation for f can be obtained.

Since (19b) is decoupled from (19a), it suffices to determine f by solving (19a) and then compute p through (19b).

4.3 “Diffusive Equation”

Solving (19a) may be cumbersome, since it is a highly nonlinear partial differential equation of the third-order in the radial derivatives of f , and it involves the mixed derivatives of f with respect to time and the radial coordinate. The scope of this section is to show that (19a) can be transformed into a pseudo-diffusion-reaction equation in J . To achieve this goal, the first step consists of the change of variables

$$f'(R, t) = \lambda_R(R, t) = \frac{RJ(R, t)}{f(R, t)\lambda_Z(t)}. \quad (20)$$

Accordingly, λ_R can be viewed as a function of J , f , λ_Z and R , where the dependence on $\lambda_Z(t)$, which is known from the outset, can be rephrased as an explicit dependence on time. Similarly, λ_Θ can be regarded as a function of f and R . Hence, the stresses P_c^{rR} and $P_c^{\vartheta\Theta}$ can be reformulated as follows:

$$P_c^{rR} = \tilde{P}_c^{rR}(J(R, t), f(R, t), \lambda_Z(t), R), \quad (21a)$$

$$P_c^{\vartheta\Theta} = \tilde{P}_c^{\vartheta\Theta}(J(R, t), f(R, t), \lambda_Z(t), R). \quad (21b)$$

By substituting the right-hand-sides of (21a) and (21b) into (19a), and performing some algebraic manipulations that account for the new definitions of stress (21a) and (21b), it is possible to define the quantities

$$\mathcal{D} := \frac{k}{\lambda_R} \frac{\partial \tilde{P}_c^{rR}}{\partial J}, \quad (22a)$$

$$-\mathcal{A}J := \frac{k}{\lambda_R} \left\{ \frac{\partial \tilde{P}_c^{rR}}{\partial f} \lambda_R + \frac{\partial \tilde{P}_c^{rR}}{\partial R} \Big|_{\text{exp}} + \frac{\tilde{P}_c^{rR} - \tilde{P}_c^{\vartheta\Theta}}{R} \right\}, \quad (22b)$$

where $[\partial(\cdot)/\partial R]|_{\text{exp}}$ represents the explicit derivative along the radial direction. Consequently, (19a) takes the form of a diffusion-advection equation in the variable J (the transported field), i.e.,

$$j = \left(\frac{\partial}{\partial R} + \frac{1}{R} \right) \left[\mathcal{D} \frac{\partial J}{\partial R} - \mathcal{A}J \right], \quad (23)$$

with \mathcal{D} and \mathcal{A} playing the role of the diffusion coefficient and advection velocity, respectively. The physical units of \mathcal{D} and \mathcal{A} , which are given by $[\mathcal{D}] = \text{length}^2/\text{time}$ and $[\mathcal{A}] = \text{length}/\text{time}$, show that these identifications are physically sound.

It is worth to mention that \mathcal{D} stems from the combination of very important physical entities. These are the permeability, which encapsulates all information about the hydraulic response of the system, and the derivative of \tilde{P}_c^{rR} with respect to J , which

is related to the acoustic tensor of the solid phase. Analogous considerations hold true for the drift velocity \mathcal{A} . In this case, however, also the term $(\tilde{P}_c^{rR} - \tilde{P}_c^{\vartheta\Theta})/R$ contributes to advection.

The coefficients \mathcal{D} and \mathcal{A} can be expressed as functions of J , f , λ_Z and R . Therefore, the diffusion-advection equation (23) is coupled with the radial deformation f , which can be determined by solving (20). In conclusion, the change of variables (20) rephrases the mathematical structure of (19a) and (19b) into the following set of new model equations:

$$f'(R, t) = \frac{RJ(R, t)}{f(R, t)\lambda_Z(t)}, \quad (24a)$$

$$j = \frac{1}{R} \frac{\partial}{\partial R} \left\{ R \left[\mathcal{D} \frac{\partial J}{\partial R} - \mathcal{A}J \right] \right\}, \quad (24b)$$

$$\frac{J}{\lambda_R} \frac{\partial p}{\partial R} = \frac{\lambda_R}{\hat{k}(J)} \left[\mathcal{D} \frac{\partial J}{\partial R} - \mathcal{A}J \right]. \quad (24c)$$

This set consists of three independent scalar equations in the three unknowns J , f and p . Clearly, the boundary conditions must be rewritten accordingly:

$$f(0, t) = 0 \quad [\text{axial symmetry}], \quad (25a)$$

$$\left(\mathcal{D} \frac{\partial J}{\partial R} - \mathcal{A}J \right) \Big|_{R=0} = 0 \quad [\text{axial symmetry}], \quad (25b)$$

$$p(R_{\text{ext}}, t) = 0 \quad [\text{from (15a)}], \quad (25c)$$

$$\tilde{P}_c^{rR}(J, f, \lambda_Z(t), R) \Big|_{R=R_{\text{ext}}} = 0 \quad [\text{from (15b)}]. \quad (25d)$$

Note that (25a) is a homogeneous Dirichlet condition on f (only one boundary condition is needed for f , since (24a) is of the first order), (25b) and (25d) express, respectively, a homogeneous Robin condition and a Dirichlet condition on J , while (25c) is a Dirichlet condition on p . Finally, the initial conditions read $f(R, 0) = R$, $J(R, 0) = 1$, and $p(R, 0) = 0$, for all $R \in [0, R_{\text{ext}}]$.

4.4 Discretisation and Results

Let $[0, T]$ be the interval of time over which the system is observed, and let $0 = t_0 < t_1 < \dots < t_N = T$ be a partition of $[0, T]$, where $\tau_n = t_n - t_{n-1}$ is the amplitude of the subinterval $[t_{n-1}, t_n] \subset [0, T]$, for $n = 1, \dots, N$, and N is the total number of such sub-intervals. Similarly, $[0, R_{\text{ext}}]$ is partitioned as $0 = R_0 < R_1 < \dots < R_M = R_{\text{ext}}$, with $\Delta_m = R_m - R_{m-1}$ being the amplitude of $[R_{m-1}, R_m] \subset [0, R_{\text{ext}}]$, for $m = 1, \dots, M$. Given a generic function q of the radial coordinate and time, the notation $q_{m,n} = q(R_m, t_n)$ indicates that q is evaluated at the point (R_m, t_n) of the space-time grid constructed above.

Due to the high non-linearity of the system, especially in \mathcal{D} and \mathcal{A} , an explicit Euler method in time is chosen for (24b). To

avoid the occurrence of numerical instabilities, the amplitudes Δ_m and τ_n , which measure, respectively, the increments in space and time, are required to satisfy the constraint $\Delta_m^2/2\tau_n \leq \mathcal{D}_{\text{ref}}$, for all $m = 1, \dots, M$, and for all $n = 1, \dots, N$, where \mathcal{D}_{ref} is a constant, referential value of the diffusion coefficient.

The discretised form of (24a)–(24c) is given by

$$f_{m,n} - f_{m-1,n} = \Delta_m \frac{R_m J_{m,n}}{f_{m,n} \lambda_Z(t_n)}, \quad (26a)$$

$$J_{m,n} - J_{m,n-1} = \tau_n \left[\frac{Q_{m,n-1} - Q_{m-1,n-1}}{\Delta_m} + \frac{Q_{m,n-1}}{R_m} \right], \quad (26b)$$

$$\frac{p_{m,n} - p_{m-1,n}}{\Delta_m} = \frac{(\lambda_{Rm,n})^2}{J_{m,n} k_{m,n}} Q_{m,n}, \quad (26c)$$

with $m = 1, \dots, M$ and $n = 1, \dots, N$. For all $p = 0, \dots, M-1$, and for all $q = 0, \dots, N$, Q_{pq} is defined as

$$Q_{p,q} = \mathcal{D}_{p,q} \frac{J_{p+1,q} - J_{p,q}}{\Delta_p} - \mathcal{A}_{p,q} J_{p,q}. \quad (27)$$

The equations have been implemented independently both in Fortran and in Matlab[®].

For the simulation of the homogeneous unconfined compression, the parameters specifying the Holmes-Mow permeability defined in (10) are given by $k_0 = 2.519 \cdot 10^{-3} \text{ mm}^2 \text{ MPa}^{-1} \text{ s}^{-1}$, $M = 4.638$, $\gamma = 0.0848$, and $\phi_{sR} = 0.2$, while the constants that characterise the Holmes-Mow hyperelastic potential (8) are taken as $\alpha_0 = 0.11 \text{ MPa}$, $\alpha_1 = 0.26$, $\alpha_2 = 0.25$, and $\beta = 0.76$. With the exception of α_1 and α_2 , whose values were assumed, all these data were taken from the experiments on bovine cartilage reported in [5]. The specimen is a cylinder of height $H = 2 \text{ mm}$ and radius $R_{\text{ext}} = 3 \text{ mm}$. Finally, the parameters defining the imposed axial stretch are the target axial displacement $u_T = 0.4 \text{ mm}$ (corresponding to a final 20% nominal strain) and the time constant $t_u = 10 \text{ s}$.

For the whole duration of the simulated experiment, and for the considered set of parameters, only relatively small variations of the volume ratio J (less than the 10%) are observed. Moreover, through most of the (normalised) radius, J remains practically uniform and equal to the initial (undeformed) value of 1, while, close to the lateral boundary, the fluid exudation causes a loss of fluid volume, which is reflected in a decrease in J (Fig. 1). Also the radial component P_c^{rR} of the constitutive part of the first Piola-Kirchhoff stress tensor (normalised to the material parameter α_0) remains virtually uniform through most of the range of the (normalised) radial coordinate, and then decreases to zero to satisfy the boundary condition of zero traction. As time goes on, the stress relaxes because of the exudation of the fluid (Fig. 2).

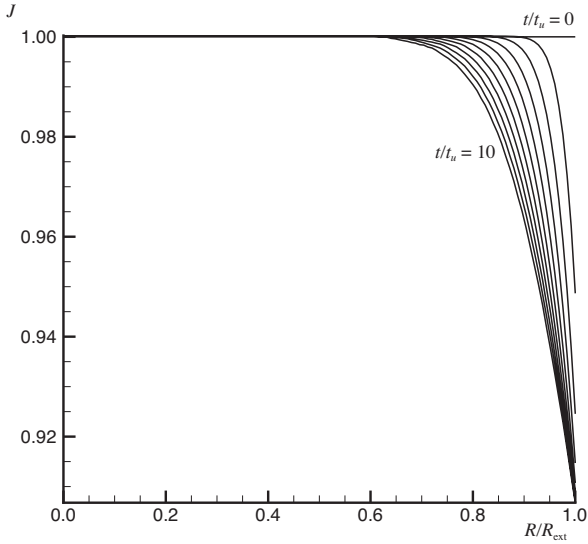


FIGURE 1. Volume ratio J vs the normalised radial coordinate R/R_{ext} . The curves are plotted for values of the normalised time $t/t_u = 0, 1, \dots, 10$.

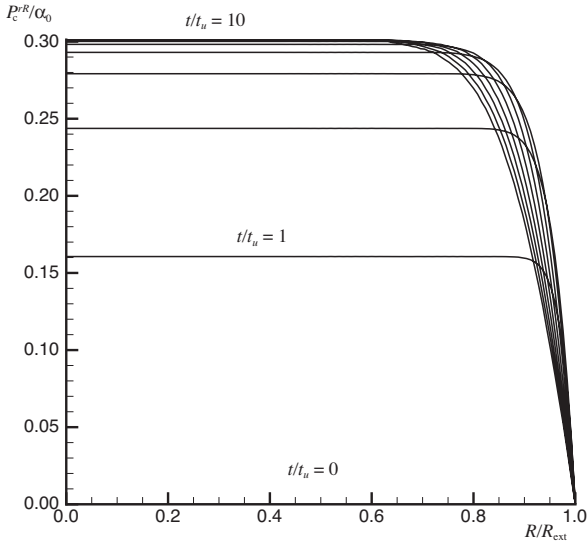


FIGURE 2. Radial component P_c^{rR} of the constitutive part of the first Piola-Kirchhoff stress tensor of the solid phase, normalised to the material parameter α_0 , vs the normalised radial coordinate R/R_{ext} . The curves are plotted for values of the normalised time $t/t_u = 0, 1, \dots, 10$.

5 Axisymmetric Confined Compression

This section focuses on another experimental test that is largely used for characterising the hydraulic and mechanical behaviour of articular cartilage: the axisymmetric confined com-

pression test. A specimen of tissue is inserted into a cylindrical, impermeable, rigid chamber and compressed by a porous, rigid piston, so that the fluid can escape through it when the specimen is compressed. In the following, confined compression is simulated in displacement control.

5.1 Specific Form of the Deformation

The solid phase of the tested biphasic medium is isotropic and “transversely homogeneous”, i.e., its material properties are allowed to vary only along the axial direction. Furthermore, due to the impermeability of the lower plate and the lateral wall of the chamber, the only non-vanishing component of the fluid velocity is along the symmetry axis of the specimen. In the usual material and spatial cylindrical coordinates $\{R, \Theta, Z\}$ and $\{r, \theta, z\}$, the deformation is given by

$$r = \chi^r(R, \Theta, Z, t) = R, \quad (28a)$$

$$\vartheta = \chi^\vartheta(R, \Theta, Z, t) = \Theta, \quad (28b)$$

$$z = \chi^z(R, \Theta, Z, t) \equiv g(Z, t), \quad (28c)$$

where χ^z has been redefined as a function g of the axial coordinate Z and time alone. The matrix representing \mathbf{F} (from which that of \mathbf{C}^{-1} can be obtained) is

$$[F_A^q](Z, t) = \text{diag}[1, 1, \lambda_Z(Z, t)], \quad (29)$$

since the radial and axial stretches are $\lambda_R = \lambda_\Theta = 1$, while the axial stretch λ_Z satisfies $J = \lambda_Z = g'$, at all points and all times, with the prime denoting partial differentiation with respect to the axial coordinate Z .

5.2 Stress and Balance Equations

The form of the deformation specified in (28a)–(28c) implies that also the matrix representing \mathbf{P}_c is diagonal, and its components can be written as

$$P_c^{rR}(Z, t) = \tilde{P}_c^{rR}(J(Z, t), Z), \quad (30a)$$

$$P_c^{\vartheta\Theta}(Z, t) = \tilde{P}_c^{\vartheta\Theta}(J(Z, t), Z), \quad (30b)$$

$$P_c^{zZ}(Z, t) = \tilde{P}_c^{zZ}(J(Z, t), Z), \quad (30c)$$

where the explicit dependence of the constitutive laws on Z has been indicated. Moreover, since all derivatives in directions other than the axial one vanish identically, and since P_c^{rR} and $P_c^{\vartheta\Theta}$ are equal to each other, the model equations (12a) and (12b) simplify

401 to

$$j = \frac{\partial}{\partial Z} \left[\frac{k}{J} \frac{\partial P_c^{zZ}}{\partial Z} \right], \quad (31a)$$

$$\frac{\partial p}{\partial Z} = \frac{\partial P_c^{zZ}}{\partial Z}, \quad (31b)$$

402 where the permeability k is now assumed to depend explicitly
403 on the axial coordinate. In this formulation, the unknowns are
404 the axial deformation g and the pressure p . If the experiment is
405 performed in displacement control, the following set of boundary
406 and initial conditions must be respected by the unknowns.

407 At the lower boundary (rigid, at rest, and impermeable),

$$g(0, t) = 0, \quad (32a)$$

$$\left(\frac{\partial p}{\partial Z}(0, t) = 0 \Rightarrow \right) \frac{\partial P_c^{zZ}}{\partial Z}(0, t) = 0. \quad (32b)$$

408 At the upper boundary (rigid, moving downward, permeable),

$$g(H, t) = H - u_T [1 - \exp(-t/t_u)], \quad (33a)$$

$$p(H, t) = 0. \quad (33b)$$

409 Furthermore, the initial conditions are given by $g(Z, 0) = Z$ and
410 $p(Z, 0) = 0$, for all $Z \in [0, H]$.

411 5.3 “Diffusive Equation”

412 As done in Section 4.3 for the case of the unconfined compression
413 test, (31a) can be reformulated in the form of a pseudo-
414 diffusion-advection equation for the volume ratio J . Indeed, the
415 constitutive definition of P_c^{zZ} leads to the relation

$$\frac{\partial P_c^{zZ}}{\partial Z} = \frac{\partial \tilde{P}_c^{zZ}}{\partial J} \frac{\partial J}{\partial Z} + \frac{\partial \tilde{P}_c^{zZ}}{\partial Z} \Big|_{\text{exp}}, \quad (34)$$

416 where the second term on the right-hand-side of (34) denotes
417 the explicit derivative of \tilde{P}_c^{zZ} with respect to the axial coordinate.
418 Thus, by introducing the notation

$$\mathcal{D} := \frac{k}{J} \frac{\partial \tilde{P}_c^{zZ}}{\partial J}, \quad (35a)$$

$$-\mathcal{A}J := \frac{k}{J} \frac{\partial \tilde{P}_c^{zZ}}{\partial Z} \Big|_{\text{exp}}, \quad (35b)$$

419 and substituting the resulting expressions into (31a), one obtains

$$j = \frac{\partial}{\partial Z} \left[\mathcal{D} \frac{\partial J}{\partial Z} - \mathcal{A}J \right]. \quad (36)$$

420 As for (23), \mathcal{D} and \mathcal{A} play the role of the diffusion coefficient
421 and advection velocity, respectively. In this case too, the condi-
422 tion (32b), although written only for P_c^{zZ} , stems from a condition
423 imposed on the overall axial stress $P^{zZ} = -p + P_c^{zZ}$.

424 Consistently with (35a) and (35b), \mathcal{D} and \mathcal{A} can be ex-
425 pressed constitutively as functions of J and Z . As for the un-
426 confined compression test, the approach based on (36) lowers by
427 one the order of the spatial derivatives of g featuring in (31a), but
428 treats J as a free unknown of the model. Therefore, the final form
429 of the model equations reads

$$\frac{\partial g}{\partial Z} = J, \quad (37a)$$

$$\frac{\partial p}{\partial Z} = \frac{\partial \tilde{P}_c^{zZ}}{\partial Z}, \quad (37b)$$

$$j = \frac{\partial}{\partial Z} \left[\mathcal{D} \frac{\partial J}{\partial Z} - \mathcal{A}J \right]. \quad (37c)$$

430 The set (37a)–(37c) comprises three independent scalar equa-
431 tions in the three unknowns g , J and p and is, thus, closed. The
432 boundary conditions must be rephrased compatibly with the new
433 formulation. In the case of a displacement-controlled confined
434 compression test, the boundary conditions become

$$g(0, t) = 0, \quad (38a)$$

$$\left(\mathcal{D} \frac{\partial J}{\partial Z} - \mathcal{A}J \right) \Big|_{Z=0} = 0, \quad (38b)$$

$$\int_0^H J(\bar{Z}, t) d\bar{Z} = H - u_T [1 - \exp(-t/t_u)]. \quad (38c)$$

$$p(H, t) = 0, \quad (38d)$$

435 which have to hold at all times $t \in [0, T]$. Equation (38b) is a
436 homogeneous Robin condition on J .

437 Since (37a) and (37b) are decoupled from (37c), they can be
438 solved *a posteriori*, once J is determined by means of (37c). In
439 particular, it is possible to directly integrate (37a) and (37b), i.e.,

$$g(Z, t) = \int_0^Z J(\bar{Z}, t) d\bar{Z}, \quad (39a)$$

$$p(Z, t) = \tilde{P}_c^{zZ}(J(Z, t), Z) - \tilde{P}_c^{zZ}(J(H, t), H). \quad (39b)$$

440 5.4 Discretisation and Results

441 The numerical solution to (37c) is determined by using cen-
442 tral differences for the space derivatives, and an ordinary differ-
443 ential equation (ODE) solver for the time derivatives [12]. The
444 computational domain $[0, H]$ is partitioned as $0 = Z_1 < \dots <$
445 $Z_M = H$, which determines $M - 1$ subintervals. In the proce-
446 dure adopted in this work, all subintervals have the same length

447 Δ . Moreover, for the sake of a lighter notation, the identification
 448 $P_c^{zZ} \equiv P$ is made. At the m th grid node, with $m = 2, \dots, (M - 1)$,
 449 the spatially discretised form of (37c) is given by

$$j_m = \frac{1}{\Delta^2} \left[\frac{k_{m+1}}{J_{m+1}} (P_{m+1} - P_m) - \frac{k_m}{J_m} (P_m - P_{m-1}) \right]. \quad (40)$$

450 Note that the nodes Z_m , with $m = 2, \dots, M - 1$, belong to the
 451 interior of the computational domain. The values J_1 and J_M ,
 452 which correspond to the boundary nodes, must be determined in
 453 compliance with the conditions (38b) and (38c). Furthermore, to
 454 maintain the second-order-accuracy of the discretisation scheme,
 455 a fictitious node $Z_0 < Z_1$ is introduced, so that the partial deriva-
 456 tive of J featuring in the Robin condition (38b) can be approx-
 457 imated by means of the central difference $(J_2 - J_0)/(2\Delta)$ [12].
 458 The ODEs (40) are then solved in time by using a stable ODE
 459 solver, with initial condition $J_m(0) = 1$, for all $m = 1, \dots, M$. All
 460 numerical simulations have been performed both in Fortran and
 461 in Matlab[®].

462 For the confined compression test, P_c^{zZ} is given by

$$P_c^{zZ} = \tilde{P}_c^{zZ}(J, Z) = \frac{1}{2}A(Z) \exp[(J^2 - 1)\beta] \frac{J^2 - 1}{J^{2\beta+1}}, \quad (41)$$

463 where $A = 4\alpha_0\beta = 4\alpha_0(\alpha_1 + 2\alpha_2)$ [5] is the aggregate elastic
 464 modulus (i.e., the stiffness in uni-axial deformation in the linear
 465 theory, given by the component L^{ZZZZ} of the (material) linear
 466 elasticity tensor \mathbb{L}), and $\alpha_0, \alpha_1, \alpha_2, \beta$ are the material constants
 467 in the Holmes-Mow hyperelastic potential (8).

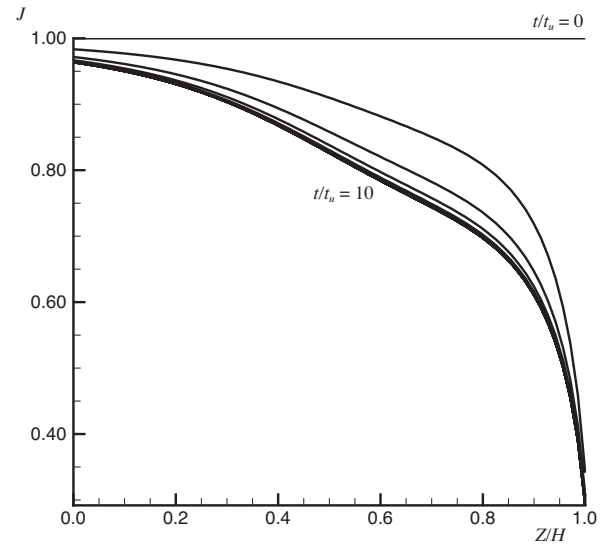
468 For this numerical implementation, the undeformed permeability k_0
 469 is obtained by extrapolating the experimental data taken from [10],
 470 and the material parameter $\alpha_0 = A/(4\beta)$ is obtained from the values
 471 of the aggregate modulus A from the experimental reported in [11].
 472 Both are expressed by third-order polynomials in the normalised depth
 473 Z/H , i.e.,

$$k_0(Z) = \left[-1.4485 \left(\frac{Z}{H}\right)^3 + 1.4813 \left(\frac{Z}{H}\right)^2 + 0.0193 \left(\frac{Z}{H}\right) + 0.1371 \right] \cdot 10^{-3} \text{mm}^2 \text{MPa}^{-1} \text{s}^{-1}, \quad (42)$$

$$\alpha_0(Z) = \left[-1.4953 \left(\frac{Z}{H}\right)^3 + 3.3255 \left(\frac{Z}{H}\right)^2 - 2.6711 \left(\frac{Z}{H}\right) + 0.8471 \right] \text{MPa}, \quad (43)$$

474 whereas all other parameters are the same as for the case of un-
 475 confined compression ($M = 4.638$, $\gamma = 0.0848$, and $\phi_{sR} = 0.2$
 476 from [5], $\alpha_1 = 0.26$ and $\alpha_2 = 0.25$, whose values are assumed,
 477 and $\beta = \alpha_1 + 2\alpha_2 = 0.76$ from [5]). In this case too, the specimen
 478 is a cylinder of initial height $H = 2$ mm and radius $R_{\text{ext}} = 3$ mm.
 479 The target value and time constant of the imposed axial displacement
 480 are $u_T = 0.4$ mm (corresponding to a final 20% nominal strain)
 481 and $t_u = 10$ s.

482 Because of the inhomogeneous material properties, the volume
 483 ratio J is inhomogeneous through the (normalised) depth of
 484 the sample also at stationary state; in particular, the much lower
 485 stiffness $\alpha_0 = A/(4\beta)$ in the superficial zone (close to $Z = 1$)
 486 makes the volumetric compression extreme for the considered
 487 overall deformation, with values of $J \simeq 0.30$ (Fig. 3). Since
 488 the pressure p must be zero on the upper boundary, the absolute
 489 value of the axial component P_c^{zZ} of the constitutive part of the
 490 first Piola-Kirchhoff stress (normalised to the value $\alpha_0(0)$ that
 491 the material parameter α_0 takes at $Z = 0$) is largest at the upper
 492 boundary and equals the absolute value of the total (normalised)
 493 stress P^{zZ} ; at the end of the test, stationary state is practically
 494 achieved, as p is zero and consequently P_c^{zZ} is uniform through-
 495 out the tissue depth (Fig. 4).



496 **FIGURE 3.** Volume ratio J vs the normalised axial coordinate Z/H .
 497 The curves are plotted for values of the normalised time $t/t_u =$
 498 $0, 1, \dots, 10$.

496 6 Discussion

497 In this work, following the lines of Armstrong et al. [4], who
 498 studied unconfined compression of isotropic homogenous cartilage
 499 under small deformations, and of Holmes and Mow [5], who
 500 studied confined compression of homogenous isotropic cartilage
 501 under large deformations, we addressed the unconfined case in
 502 the large-deformation setting, and the confined case by remov-
 503 ing the hypothesis of homogeneity, thereby allowing some of the
 504 material properties to vary along the axis of compression. In both
 505 the cases of unconfined and confined compression, we reduced
 506 the problem to a diffusion-advection equation in J , which was

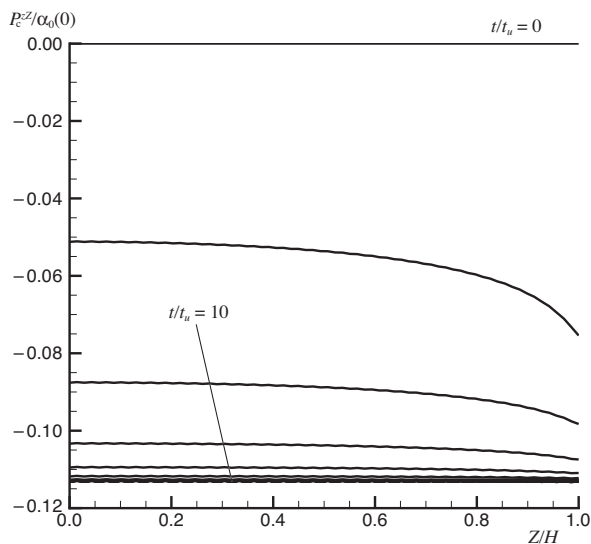


FIGURE 4. Axial component P_c^Z of the constitutive part of the first Piola-Kirchhoff stress tensor of the solid phase, normalised to the value $\alpha_0(0)$ of the material parameter α_0 at $Z = 0$, vs the normalised axial coordinate Z/H . The curves are plotted for values of the normalised time $t/t_u = 0, 1, \dots, 10$.

regarded as the relevant kinematical variable. A result similar to the diffusion-advection equation (36) of the confined case was obtained in [12]. There are, however, two major differences between the two approaches. Firstly, the model analysed in [12] was homogeneous and, consequently, could not obtain the advection “velocity” \mathcal{A} . This “velocity”, indeed, arises because of the inhomogeneity of the constitutive law of the axial stress. Secondly, in [12], tissue remodelling (an anelastic process) was considered, and the hydraulic and mechanical behaviour of the specimen was studied in the elastic range subsequent remodelling.

Although more precise descriptions of articular cartilage have been given [9, 15, 16], where the inhomogeneity and anisotropy of the tissue induced by the presence of the collagen fibres have been considered, and more general constitutive models can be conceived to include effects such as growth and remodelling (cf., e.g., [17, 18]), the mathematical formulation presented in this work is based on the non-linear biphasic (solid-fluid) model. Since we are working with an established theory, and the only “arbitrary” choice is that on the constitutive equations, we believe that, by fitting parameters, the vast majority of experimental confined or unconfined tests could validate our numerical simulations. However, it is clear that homogeneous and isotropic cartilage does not exist and therefore the unconfined case would certainly be a rather artificial fitting of material parameters. Moreover, to the best of our knowledge, there is *no* confined compression test in which both the elastic properties

and the permeability have been evaluated. Indeed, the permeability measurements performed by Maroudas and Bullough [10] do not involve any compression test and, conversely, the compression tests performed by Schinagl et al. [11] do not involve any permeability measurement. Specifically, the inhomogeneous permeability measurements performed by Maroudas and Bullough [10] are the only ones we are aware of. Therefore, we cannot infer that our results can have direct experimental validation. As far as a comparison with other computational models is concerned, the theoretical derivation of our model has been obtained by simplifying the theory of biphasic mixtures comprising an inviscid fluid and a hyperelastic solid material under the assumption that both phases are incompressible. In this respect, our theoretical results are expected to be consistent with those obtained by the inhomogeneous and anisotropic theory, if the appropriate model reductions are made.

One of the limitations of the method presented here is the isotropy of the material properties. Indeed, mostly due the presence of the collagen fibres, articular cartilage exhibits anisotropic behaviour in both its elastic properties (see, e.g., [9, 16, 19]) and permeability (see, e.g., [8, 9, 15, 16, 20]). However, the anisotropy of the tissue was not taken into account here, since the purpose of this work is to show how much information about the mechanical and hydraulic behaviour of the tissue can be extracted also from much simpler models, which do not require elaborated numerical procedures such as the Finite Element Method. Note that neither the fluid inside the cells, nor the intrafibrillar fluid [21, 22] are explicitly accounted for in the presented model. Considering these fluids, along with the ions dissolved in them, and their interaction with all the other constituents of the tissue would call for a full electro-chemo-mechanical approach, whose solution would require the employment of sophisticated numerical procedures, especially when large deformations occur. Such a detailed level of modelling is out of the scopes of this paper. The proposed approach is valid also in more complex cases, as long as the further complication is in the non-linearity of the constitutive laws, but ceases to be applicable when the added complication breaks one or more symmetries of the problem. In this case, Finite Element methods often become indispensable.

In our opinion, the advantage of using Finite Differences against Finite Element methods for the problems at hand lies in the fact that the problem reduction shown in the manuscript makes it sufficient to employ one-dimensional grids for solving the model equations in a sufficiently stable, efficient and accurate way, while keeping the computational costs at an acceptable level. This is due to the fact that each of the considered problems is reduced to a set of partial differential equations in which the space dependence appears solely in the partial derivatives with respect to the radial coordinate (in the unconfined compression) or to the axial coordinate (in the confined compression).

The importance of this work is, in fact, in the possibility of testing a given material behaviour (or, more precisely, the

isotropic version of a material behaviour) in a non-trivial, biphasic, large deformation setting. This means that the result of the Finite Element implementation of a user-defined material can be tested against the proposed method, which gives full control on all physical quantities, since it is based directly on the governing differential equations.

Acknowledgements

Alberta Innovates - Technology Futures (Canada) [SF], Alberta Innovates - Health Solutions (Canada) [SF], the Natural Sciences and Engineering Research Council of Canada [SF], the Start-up Packages and PhD Program Project, co-funded by Regione Lombardia (Italy) [CG], and the Progetto Giovani GNFM 2014 funded by the Italian National Group of Mathematical Physics [CG].

REFERENCES

[1] Torzilli, P. A., and Mow, V. C., 1976. "On the fundamental fluid transport mechanisms through normal and pathological articular cartilage during function - I - the formulation". *J. Biomech.*, **9**, pp. 541–552.

[2] Torzilli, P. A., and Mow, V. C., 1976. "On the fundamental fluid transport mechanisms through normal and pathological articular cartilage during function - II - the analysis, solution and conclusions". *J. Biomech.*, **9**, pp. 587–606.

[3] Mow, V. C., Kuei, S. C., Lai, W. M., and Armstrong, C., 1980. "Biphasic creep and stress relaxation of articular cartilage in compression: Theory and experiments". *J. Biomech. Eng.*, **102**, pp. 73–84.

[4] Armstrong, C. G., Lai, W. M., and Mow, V. C., 1984. "An analysis to unconfined compression of articular cartilage". *J. Biomech.*, **106**, pp. 165–173.

[5] Holmes, M. H., and Mow, V. C., 1990. "The nonlinear characteristics of soft gels and hydrated connective tissues in ultrafiltration". *J. Biomech.*, **23**, pp. 1145–1156.

[6] Federico, S., Grillo, A., Giaquinta, G., and Herzog, W., 2009. "A semi-analytical solution for the confined compression of hydrated soft tissue". *Meccanica*, **44**, pp. 197–205.

[7] Grillo, A., Federico, S., Wittum, G., Imatani, S., Giaquinta, G., and Mićunović, M. V., 2009. "Evolution of a fibre-reinforced growing mixture". *Nuovo Cimento C*, **32C**, pp. 97–119.

[8] Federico, S., and Grillo, A., 2012. "Elasticity and permeability of porous fibre-reinforced materials under large deformations". *Mech. Mat.*, **44**, pp. 58–71.

[9] Tomic, A., Grillo, A., and Federico, S., 2014. "Poroelectric materials reinforced by statistically oriented fibres - numerical implementation and application to articular cartilage". *IMA J. Appl. Math.*, **79**, pp. 1027–1059.

[10] Maroudas, A., and Bullough, P., 1968. "Permeability of articular cartilage". *Nature*, **219**, pp. 1260–1261.

[11] Schinagl, R. M., Gurskis, D., Chen, A. C., and Sah, R. L., 1997. "Depth-dependent confined compression modulus of full-thickness bovine articular cartilage". *J. Orthop. Res.*, **15**, pp. 499–506.

[12] Grillo, A., Giverso, C., Favino, M., Krause, R., Lampe, M., and Wittum, G., 2012. "Mass transport in porous media with variable mass". In *Numerical Analysis of Heat and Mass Transfer in Porous Media — Advanced and Structured Materials*, J. M. P. Q. Delgado, A. G. B. de Lima, and M. V. d. Silva, eds. Springer-Verlag, Berlin Heidelberg, pp. 27–61.

[13] Madeo, A., dell’Isola, F., and Darve, F., 2013. "A continuum model for deformable, second gradient porous media partially saturated with compressible fluids". *J. Mech. Phys. Solids*, **61**, pp. 2196–2211.

[14] Ateshian, G. A., and Weiss, J. A., 2010. "Anisotropic hydraulic permeability under finite deformation". *J. Biomech. Eng.*, **132**, p. 111004.

[15] Federico, S., and Herzog, W., 2008. "On the anisotropy and inhomogeneity of permeability in articular cartilage". *Biomech. Model. Mechanobiol.*, **7**, pp. 367–378.

[16] Pierce, D. M., Ricken, T., and Holzapfel, G. A., 2013. "A hyperelastic biphasic fibre-reinforced model of articular cartilage considering distributed collagen fibre orientations: continuum basis, computational aspects and applications". *Comput. Meth. Biomech. Biomed. Eng.*, **16**, pp. 1344–1361.

[17] Lekszycki, T., and dell’Isola, F., 2012. "A mixture model with evolving mass densities for describing synthesis and resorption phenomena in bones reconstructed with bio-resorbable materials". *Z. Angew. Math. Mech.*, **92**, pp. 426–444.

[18] Andreaus, U., Giorgio, I., and Madeo, A., 2015. "Modeling of the interaction between bone tissue and resorbable biomaterial as linear elastic materials with voids". *Z. Angew. Math. Phys.*, DOI:10.1007/s00033-014-0403-z.

[19] Wilson, W., Huyghe, J. M., and van Donkelaar, C. C., 2007. "Depth-dependent compressive equilibrium properties of articular cartilage explained by its composition". *Biomech. Model. Mechanobiol.*, **6**, pp. 43–53.

[20] Federico, S., and Herzog, W., 2008. "On the permeability of fibre-reinforced porous materials". *Int. J. Solids Struct.*, **45**, pp. 2160–2172.

[21] Loret, B., and Simoes, F. M. F., 2004. "Articular cartilage with intra- and extracellular waters: a chemo-mechanical model". *Mech. Mat.*, **36**, pp. 515–541.

[22] Loret, B., and Simoes, F. M. F., 2005. "A framework for deformation, generalized diffusion and growth in multi-species multi-phase biological tissues". *Eur. J. Mech. A/Solids*, **24**, pp. 757–781.